CHEMISTRY, PHYSIOLOGY

Correction for "Glyconanoparticles allow pre-symptomatic in vivo imaging of brain disease," by Sander I. van Kasteren, Sandra J. Campbell, Sébastien Serres, Daniel C. Anthony, Nicola R. Sibson, and Benjamin G. Davis, which appeared in issue 1, January 6, 2009, of *Proc Natl Acad Sci USA* (106:18–23; first published December 23, 2008; 10.1073/pnas.0806787106).

The authors note that due to a printer's error, the affiliation information for Sébastien Serres and Nicola R. Sibson appeared incorrectly. The correct affiliation is "CR-UK/MRC Gray Institute for Radiation Oncology and Biology." The corrected affiliation line appears below.

[a]Department of Chemistry, Chemistry Research Laboratory, University of Oxford, Mansfield Road, Oxford, OX1 3TA, United Kingdom; [b]Department of Pharmacology, University of Oxford, Mansfield Road, Oxford, OX1 3QT, United Kingdom; and [c]CR-UK/MRC Gray Institute for Radiation Oncology and Biology, Radiobiology Research Institute, University of Oxford, Churchill Hospital, Oxford, OX3 7LJ, United Kingdom

www.pnas.org/cgi/doi/10.1073/pnas.0900259106

NEUROSCIENCE, COMPUTER SCIENCES

Correction for "The minimum information principle and its application to neural code analysis," by Amir Globerson, Eran Stark, Eilon Vaadia, and Naftali Tishby, which appeared in issue 9, March 3, 2009, of *Proc Natl Acad Sci USA* (106:3490–3495; first published February 13, 2009; 10.1073/pnas.0806782106).

The authors note that due to a printer's error, an incorrect version of this article was posted online. The online version has been replaced. The print version is correct.

www.pnas.org/cgi/doi/10.1073/pnas.0901850106

Glyconanoparticles allow pre-symptomatic in vivo imaging of brain disease

Sander I. van Kasteren[a], Sandra J. Campbell[b], Sébastien Serres[c], Daniel C. Anthony[b,1], Nicola R. Sibson[c,1], and Benjamin G. Davis[a,1]

[a]Department of Chemistry, Chemistry Research Laboratory, University of Oxford, Mansfield Road, Oxford, OX1 3TA, United Kingdom; [b]Department of Pharmacology, University of Oxford, Mansfield Road, Oxford, OX1 3QT, United Kingdom; and [c]Cancer Research United Kingdom, Medical Research Council, and Gray Institute for Radiation Oncology and Biology, Radiobiology Research Institute, University of Oxford, Churchill Hospital, Oxford, OX3 7LJ, United Kingdom

Edited by Robert Langer, Massachusetts Institute of Technology, Cambridge, MA, and approved November 20, 2008 (received for review July 14, 2008)

Initial recruitment of leukocytes in inflammation associated with diseases such as multiple sclerosis (MS), ischemic stroke, and HIV-related dementia, takes place across intact, but activated brain endothelium. It is therefore undetectable to symptom-based diagnoses and cannot be observed by conventional imaging techniques, which rely on increased permeability of the blood–brain barrier (BBB) in later stages of disease. Specific visualization of the early-activated cerebral endothelium would provide a powerful tool for the presymptomatic diagnosis of brain disease and evaluation of new therapies. Here, we present the design, construction and in vivo application of carbohydrate-functionalized nanoparticles that allow direct detection of endothelial markers E-/P-selectin (CD62E/CD62P) in acute inflammation. These first examples of MRI-visible glyconanoparticles display multiple copies of the natural complex glycan ligand of selectins. Their resulting sensitivity and binding selectivity has allowed acute detection of disease in mammals with beneficial implications for treatment of an expanding patient population suffering from neurological disease.

carbohydrates | MRI | multiple sclerosis | selectins

Magnetic resonance imaging (MRI) is now the most widely-used imaging method for the study of neurologic human disease. Antibody-mediated detection of broad-spectrum inflammation biomarkers, such as VCAM-1 (1, 2), is not applicable to brain disease where alternative brain-specific markers exist (3, 4). In addition, previous attempts to detect inflammation (5–8) or to target selectin up-regulation with antibodies and small molecules in vivo have failed (8) or were shown only limited contrast enhancements at best (5–7), and none have been applied to validated models of brain disease, such as the MS model MOG-EAE (9–11) or the ET-induced focal stroke model (12–14). The carbohydrate-binding transmembrane proteins CD62E (E-selectin) and CD62P (P-selectin) are up-regulated as part of the host response to injury or disease where they play a key role in the initial tether-roll phase of the homing of leukocytes to sites of inflammation; the brain also utilizes the CD62 proteins (15), and they consequently offer an ideal, to date underexploited, biomarker for brain disease diagnosis (4).

Our strategy for detecting the CD62 proteins exploited their affinity for their cognate ligand molecule type, carbohydrates. This approach therefore necessitated precise, chemically-synthesized carbohydrate ligands to mediate CD62 binding and detection. Nano-sized particles(16–20) have been functionalized with carbohydrates for the elegant in vitro study of carbohydrate-mediated interactions, such as those mediating marine sponge interactions(17). The platforms for these particles have focused on nano-sized gold (17–19) and cadmium sulfide (CdS) (19–21). Although these are often highly convenient and flexible, they also have disadvantages, such as the toxicity (22) of CdS-based fluorescent quantum dots and the ligand-lability of gold clusters (23, 24), which is exacerbated in biological media (25). The use of glycosylated contrast agents, until now, has been limited to T_1-type reagents that rely on water exchange in their inner coordination sphere (26–30). They bring with them disadvantages of low sensitivity and low avidity for carbohydrate-binding protein targets since they display low carbohydrate copy numbers(31). Consequently, such agents do not fully exploit the cluster glycoside effects prevalent in carbohydrate-protein interaction (31–34), which is known to powerfully enhance often weak single carbohydrate ligand interactions. Here, we describe the design and creation of a T_2-type glyconanoparticle reagent **GNP-sLe^x** that was specifically targeted to CD62 (E- and P-selectin) by virtue of its decoration with many (millions) of copies of the relevant, complex, cognate, glycan ligand sialyl Lewis^X (sLe^x) normally found on most bloodborne leukocyte subpopulations. **GNP-sLe^x** was selected from a number of glyconanoparticles of increasing carbohydrate complexity constructed on a platform of cross-linked amine-functionalized iron oxide (35, 36). These nanoparticles circumvent problems of low contrast; their high iron content conveys upon them far superior relaxation (and hence detection) effects compared with T_1-agents (37–39).

Results and Discussion

The following features of the construction of the nanoparticles, including **GNP-sLe^x,** were key (Fig. 1):

1. Ready access to a high-Fe-content nanoparticular platform. An alkali suspension of iron oxide-dextran colloidal was treated sequentially with epichlorohydrin and ammonia (37, 40). The resulting cross-linked, amine-functionalized dextran-coated particle, amine nanoparticle (**NH_2-NP**), provided a versatile and safe platform for the incorporation of multiple copies of targeting glycans.
2. Multivalent nanoparticular display. Chemical assay through "Fmoc-numbering" (41) revealed high levels of amine groups per particle in **NH_2-NP** that in turn allowed the display of large numbers (10^5 to 10^7) of sugars per particle to fully exploit the clustering of selectin receptors on inflamed endothelia.
3. The development of a "masked" chemical linker group, specifically SCM (Fig. 1), that could be carried throughout the carbohydrate-assembly synthesis: Attachment of glycans to **NH_2-NP** required an amine-reactive linker group. However, the manipulation of a linker precursor to generate an active linker after synthesis of a complex glycan often results in low efficien-

Author contributions: S.I.v.K., D.C.A., N.R.S., and B.G.D. designed research; S.I.v.K., S.J.C., and S.S. performed research; S.I.v.K., S.J.C., S.S., D.C.A., N.R.S., and B.G.D. analyzed data; and S.I.v.K., D.C.A., N.R.S., and B.G.D. wrote the paper.

The authors declare no conflict of interest.

This article is a PNAS Direct Submission.

Freely available online through the PNAS open access option.

[1]To whom correspondence may be addressed. E-mail: daniel.anthony@pharm.ox.ac.uk, nicola.sibson@rob.ox.ac.uk, or ben.davis@chem.ox.ac.uk.

This article contains supporting information online at www.pnas.org/cgi/content/full/0806787106/DCSupplemental.

www.pnas.org/cgi/doi/10.1073/pnas.0806787106

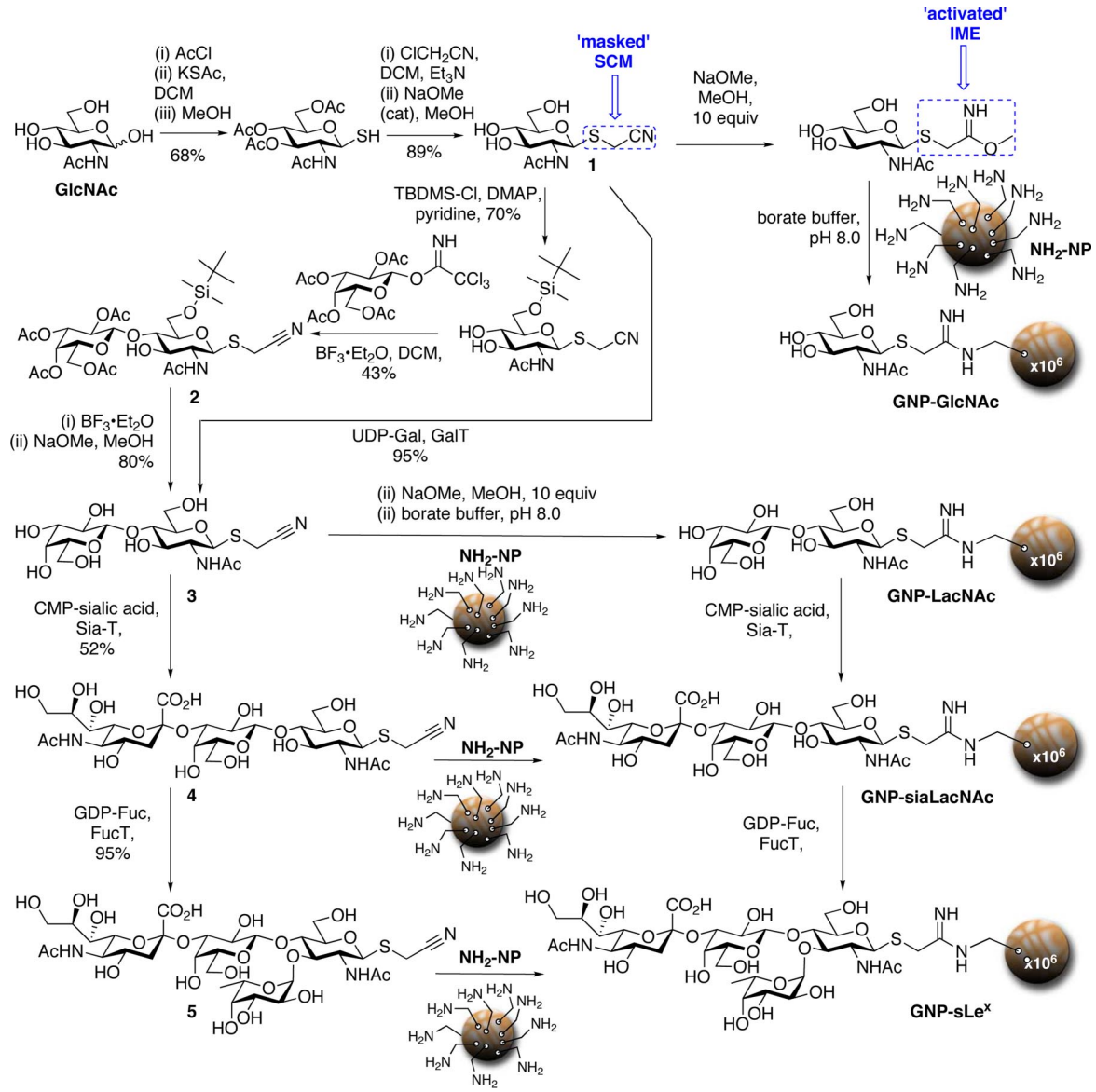

Fig. 1. Design and construction of MRI-active GlycoNanoParticles for in vivo inflammation detection. Use of a masked SCM group in a combined chemo-enzymatic synthetic strategy allowed ready access to the required complex oligosaccharide reagents and the corresponding GNPs modified with mono (GNP-GlcNAc), di- (GNP-LacNAc), tri- (GNP-siaLacNAc), and tetra-saccharides (GNP-sLe^x).

cies and reduced modification yields. We discovered that the *S*-cyanomethyl (SCM) (S—CH_2—CN) functional group could be used at the anomeric center of sugars not only as a protecting group, to aid control in the synthesis, but also a masked linker. Its dual chemical character allowed the SCM group to be introduced early in a given synthetic scheme and then selectively "unmasked" or activated by conversion to the corresponding reactive chemical group 2-imido-2-methoxy-ethyl (IME) (S—CH_2—C(NH)OCH_3) (42–45). This was accomplished cleanly, at will, before any amine-modification reaction simply by pretreatment with sodium methoxide. Importantly, this method was made possible by the discovery that substoichiometric levels of methoxide would cleanly allow manipulation of glycan protecting groups (acetyl groups) while leaving the masked linker cyanomethyl group intact (see SI).

These key discoveries together allowed the SCM-containing precursor **1** (Fig. 1) to be transformed using a series of highly stereo- and regio-selective, chemical and enzymatic glycosylation steps to assemble complex glycan reagents **2–5** in good yields and with minimal recourse to protecting group chemistry (see SI). The flexibility of the resulting synthetic method (Fig. 1) allowed the construction not only of a nanoparticle containing the tetrasaccharide **GNP-sLe^x**, but also truncated, less complex, variants incorporating mono-, di- and tri-saccharides (**GNP-GlcNAc**, **GNP-LacNAc**, and **GNP-siaLacNAc**, respectively).

The GNPs were thoroughly characterized (see SI). Chemical resorcinol (46) and fluorescamine (47) assays and enzymatic sialic acid quantification (48) revealed incorporation of 10^5 to 10^7 copies of sLe^X and the other glycans per particle (≈20 nmol·mg^{-1}); glycan display levels were advantageously fine-tuned simply through variation of reaction conditions. Moreover, the flexibility of the platform approach also allowed the GNPs to be simultaneously fluorescently labeled [using fluorescein isothiocyanate (FITC)] to allow for post mortem immunohistochemical analysis. Dynamic LASER-light scattering analysis of all particles revealed the desired nm-μm size-range; measurements before and after modifications also indicated no significant size change during reagent reaction. Further-

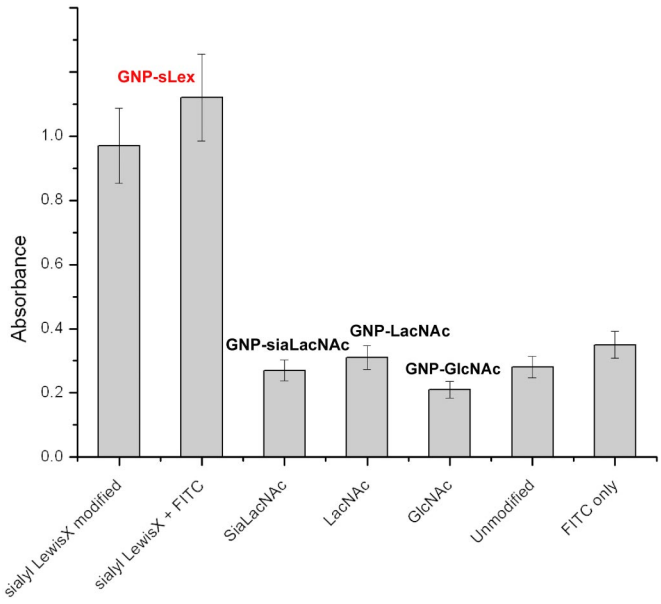

Fig. 2. In vitro binding GNPs to rat E-selectin. Access to a range of glyco-NPs of increasing complexity allowed precise determination of ligand required for biomarker targeting. Only sialyl Lewis^X (sLe^X)-modified particles (GNP-sLe^x) show biomarker binding to rat *E*-selectin-human IgG-Fc chimera above background. The presence of an additional FITC-label on the particle does not affect binding.

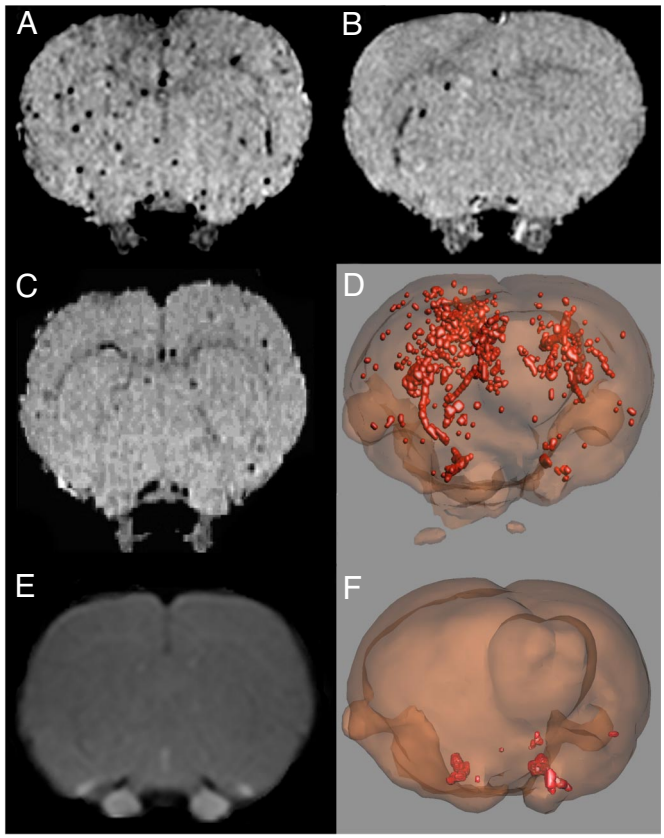

Fig. 3. MRI Imaging of GNP-sLe^x. In vivo detection of GNPs after intracerebral injection of either 100 ng of IL-1β (*A* and *C*), or 10 ng of IL-1β (*B* and *D*). Negligible detection using a control of unmodified particles after injection of 100 ng of IL-1β (*C*) highlights the sugar dependency and hence the key role of glycans in this molecular imaging. Three-dimensional volumetric maps of GNP-sLe^x binding (red) after injection of 10 ng of IL-1β (δ) or after only saline as a control (ϕ) shows that use of GNP-sLe^x even allows inflamed vascular architecture to be directly discerned and that background binding in the absence of inflammation is minimal. A T_1-weighted image (*E*) acquired at 5.5h after intraceberal injection of 1 mg of IL-1β and 10 min after i.v. injection of 100 mL of Gd-DTPA to verify lack of blood–brain barrier breakdown at the end of the GNP protocol. (See also SI for a movie of 3D reconstruction.) Views are from the front depicting left brain on the right hand side.

more, particle size could also be controlled using appropriate reaction conditions (see SI). In this way, key parameters of GNP size, glycan identity and display levels could be systematically varied and the effects probed.

Next, biomarker-particle interactions were assessed in proof-of-principle experiments that determined the critical effect of increasing glycan complexity. Little or no binding above background was observed for NPs displaying multiple copies of truncated glycan structures that contain only mono-, di-, or tri-saccharides: **GNP-GlcNAc**, **GNP-LacNAc**, and **GNP-siaLacNAc** (Fig. 2). However, **GNP-sLe^x**, which displays the CD62E (*E*-selectin) tetrasaccharide ligand sialyl Lewis^X, showed strong and selective binding to *E*-selectin-*Fc* chimera protein in in vitro biomarker binding assays(49). Moreover, binding efficiency was not significantly reduced by the additional presence of fluorescent (FITC)-labeling in the NPs. Biomarker targeting using, for example, antibodies, can be associated with broad but sometimes poorly selective detection; these results with **GNP-sLe^x** not only confirmed specific ligand-induced biomarker (CD62E, *E*-selectin) targeting, but also gave strong confirmation of the exquisite selectivity and fine-control that we hoped to achieve with these chemically-constructed targeting ligands.

This targeting and imaging ability of the nanoparticles was next tested in vivo. Selectin expression on activated endothelium in the brain was induced by microinjection of 100 ng (Fig. 3*A*) or 10 ng (Fig. 3 *B* and *D*) of interleukin-1β into the left striatum of a rat. These doses caused specific but widespread activation of the brain microvasculature with a bias toward the left hemisphere. Importantly, this cytokine has been shown to activate the endothelium at early time points without causing blood–brain barrier (BBB) breakdown.(5, 50, 51) Three hours after after intracerebral injection of 100 ng of IL-1β, animals were injected systemically with either **GNP-sLe^X** (n = 3) or control non-targeted, unfunctionalized (**control-NP**, CLIO, n = 3). Subsequently, a 3D gradient-echo T_2*-weighted pulse sequence, with 120 μm isotropic resolution, was used to determine the presence of **GNP-sLe^x** particles; images (Fig. 3*A*) clearly showed numerous pixels with reduced signal intensity in animals injected intracerebrally with IL-1β thereby allowing sensitive and direct particle detection. Considerably greater accumulation of **GNP-sLe^x** was observed in the left cranial hemisphere, around the site of inflammation induction. To test sensitivity of the **GNP-sLe^x** particles to lower dose interleukin-1β injection, an additional animal was injected with 10 ng in the same way. Again binding of the **GNP-sLe^x** particles was evident in the injected hemisphere, although fewer than with 100 ng of interleukin-1β, and in this case almost no particles were found in the contralateral hemisphere (Fig. 3 *B* and *D*). Very few particles were observed in animals injected with 100 ng of interleukin-1β and, subsequently, either unmodified **control-NP** particles (Fig. 3*C*) or the GNP variant **GNP-LacNAc** bearing a truncated glycan structure. Similarly, control animals injected intracerebrally with the same volume of vehicle (sterile saline) and subsequently with **GNP-sLe^x** (n = 3), showed very little particle retention (Fig. 3*F*). 3D-reconstructions (see movie in SI) of **GNP-sLe^x** accumulation revealed imaging resolution sufficient even to allow the detailed architecture of the activated vasculature to be determined (Fig. 3*D*), and confirmed the lack of **GNP-sLe^x** retention in control animals (Fig. 3*F*). Moreover, a T_1-weighted image (Fig. 3*E*) acquired at 5.5h after intraceberal injection of 1 mg of IL-1β and 10 min after i.v. injection

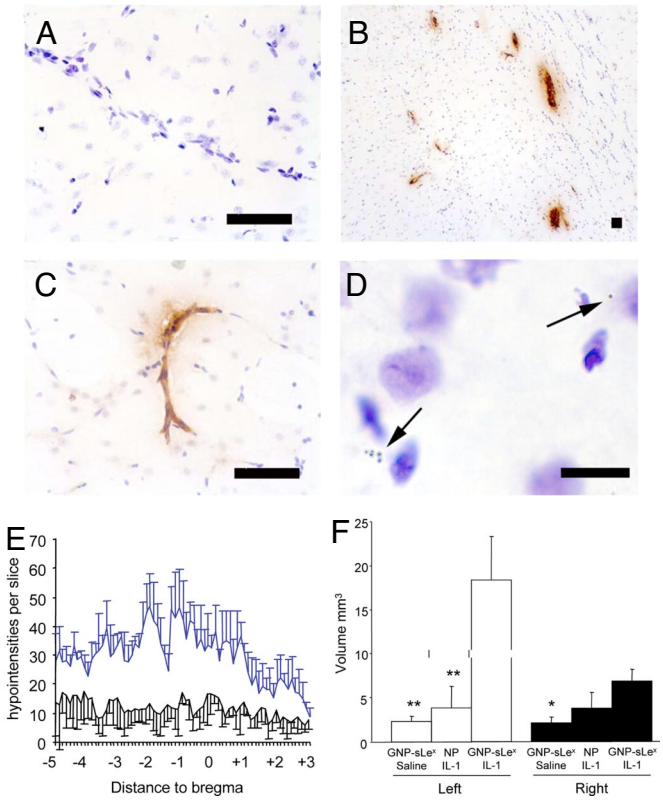

Fig. 4. Localisation of Nanoparticles. (*A*) No nonglycosylated FITC-NP could be detected by anti-FITC immunohistochemistry in the vasculature 4 h after the injection of IL-1β into the brain. (*B*) In contrast, GNP-sLe^x-FITC (brown stain) localized to the vasculature in the IL-1β injected brain. (*C*) A higher-power image of the GNP-sLe^x-FITC in a vessel in the injected striatum. (*D*) A high power photomicrograph of GNP-sLe^x particles (arrows) in the vasculature. All tissue sections were counterstained with cresyl violet. (Scale bars: *A*–*C*, 50 μm; *D*, 10 μm.) (*E*) The mean ($\pm$ SD) number of hypointensities in the left hemisphere on T_2*-weighted MR images, relative to bregma, 4–5 h after the injection of 100 ng of IL-1β into the brain and $\approx$2h after injection of the targeted GNPs or un-modified NPs: unfunctionalized control-NP; black line, and GNP-sLe^x; blue line. (*F*) Total voxel volume in both hemispheres for inflamed brain with GNP-sLe^x compared with controls of GNP-sLe^x in uninflamed brain (saline injection) and unfunctionalized particle NP. ANOVA + Bonferoni. **, $P < 0.01$; *, $P < 0.05$.

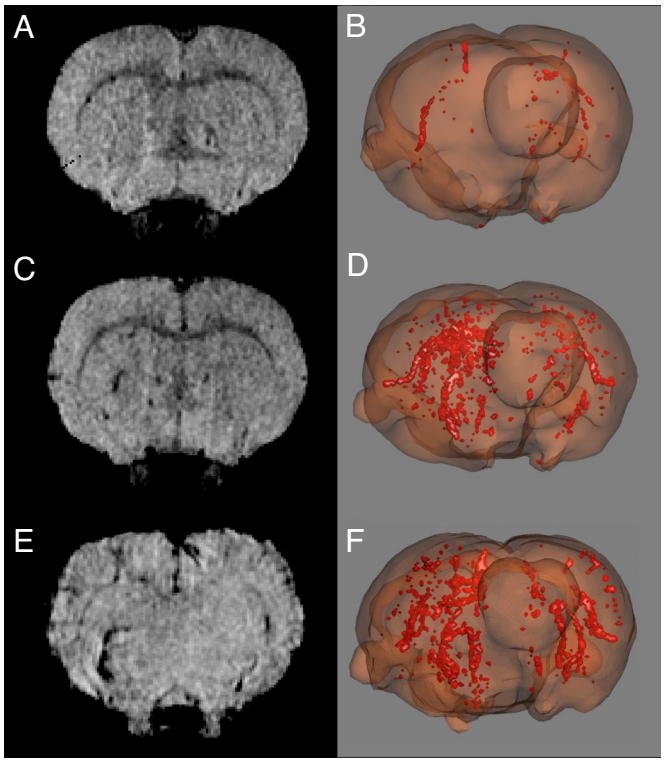

Fig. 5. Use of nanoparticles in disease detection. Selected images taken from the T_2*-weighted 3D datasets (*A*, *C*, and *E*) and 3D reconstructions of the accumulation of contrast agent (*B*, *D*, and *F*) reveal that GNP-sLe^x enables clear detection of lesions in clinically-relevant models of MS (*C* and *D*) (MOG-EAE, see SI) and stroke (*E* and *F*) (ET-1 induced, see SI) in contrast to unfunctionalized control-NP (*A* and *B*). Importantly, use of a gadolinium-based contrast agent Gd[DTPA-BMA] (Omniscan) in spin-echo T_1-weighted images to assess blood–brain barrier (BBB) permeability (*G*) and regional cerebral blood volume (rCBV) (*H*) failed to detect the presence of pathology. (See SI for movies of 3D reconstruction.) Views are from the front depicting left brain on the right hand side.

of 100 μL of T_1-agent Gd-DTPA verified a lack of blood–brain barrier breakdown at the end of the **GNP** protocol.

Quantitative analysis of the **GNP-sLe^x** showed a clear left-over-right hemisphere bias of accumulation, again consistent with the site of IL-1β inflammation induction (Fig. 4*E*). In contrast, no difference in the presence of **GNP-sLe^x** was detected between the two hemispheres of the control animals. Automatic segmentation by an operator blinded to the origin of all data also allowed contrast volume quantification (Fig. 4*F*) and the determination of "hypointensity volumes" (Fig. 4*F*), which showed that significantly more **GNP-sLe^x** is bound after IL-1β injection compared with an injection of saline control. A similar significant difference was also demonstrated between **NP** and **GNP-sLe^x** particles (Fig. 4*F*). In the IL-1β-injected animals, the area of increased **GNP-sLe^x** accumulation extended throughout much of the forebrain, from the level of the hippocampus ($\approx$2.5 mm posterior to Bregma) through to the level of the prelimbic cortex ($\approx$2.5 mm anterior to Bregma) (Fig. 4*E*) (52). Furthermore, analysis of the total volume of detected voxels in inflamed brain (Fig. 4*F*) showed significant enhancement over controls (Fig. 4*F*).

Key features of this detection method stand out. Strikingly, at the time point studied here (**GNP-sLe^x** injected 2.5–3.0 h after IL-1β; MRI 4.0–5.0 h after IL-1β) no detectable changes were evident using other MRI methods. This GNP-MRI method advantageously detects CD62E as a biomarker that is displayed on the "blood side" of the blood–brain barrier (BBB) but is indicative of pathology on the 'brain side'. As a result, not only are the GNPs cleared efficiently postdetection, there was also no BBB breakdown in this model, which can be seen with conventional contrast agents such as Gd-DPTA. No GNP toxicity was observed in any of the models.

This detection of IL-1β-induced inflammatory lesions in brain provided valuable confirmation of striking sensitivity in a model that allowed study of the acute activation of the brain endothelium in the absence of any other, potentially confounding factors such as BBB breakdown or leukocyte recruitment. However, to determine whether GNPs would be as sensitive in detecting pathology in other, clinically relevant, animal models of human neuropathology, we tested these particles in both a chronic focal MS-like lesion that is no longer Gd-enhancing (Fig. 5 *A*–*D*), and in an endothelin (ET)-induced focal stroke (12, 13, 53), which is reminiscent of lacunar infarcts (Fig. 4 *E*–*H*). Both such lesions present particular difficulties for neuroradiologists in accurately assessing lesion load and activity by MRI.

The MOG-EAE (myelin oligodendrocyte glycoprotein-experimental autoimmune encephalomyelitis) model (9–11) provides a stringent test of MS detection. Twenty-one days after the injection of recombinant cytokines into the corpus callosum, which initiated MS-like MOG-EAE lesion ($n = 3$), **GNP-sLe^x** revealed the clear presence of chronically activated brain endothelium in the region of, and immediately adjacent to, the site of the focal MS-like lesion (Fig. 5 *C* and *D* and SI). The asymmetric detection observed

with **GNP-sLe^x** particles was not seen when the **control-NP** were injected into other focal MOG-EAE animals ($n = 2$) (Fig. 5 *A* and *B*). No abnormalities were detected on T_1-weighted images post-Gd[DTPA-BMA] (see SI) confirming that the BBB was intact and that conventional imaging approaches would not have revealed such on-going pathology.

The ability of **GNP-sLe^x** to detect brain disease events was tested next in a model of stroke (12, 13, 53). Between 2.5 and 3.5 h after the induction of a focal stroke **GNP-sLe^x** particles specifically bound and clearly detected activated endothelium, both at the primary injury site and even at sites of secondary damage in the contralateral hemisphere (Fig. 5 *E* and *F* and SI). Importantly, the ET-1-induced infarct was not associated with any BBB breakdown (Fig. 5*G*) or an asymmetric rCBV (regional cerebral blood volume) (Fig. 5*H*), thus highlighting the ability **GNP-sLe^x** to detect damage in instances when other standard MRI methods fail. Moreover, the latter finding demonstrated that accumulation of **GNP-sLe^x** was not a function of reduced CBV.

These tests in varied and clinically relevant animal models of brain disease demonstrated that **GNP-sLe^x** particles can reveal the presence of pathology that is not visible with conventional MRI methods. The in vivo MRI data were corroborated by direct **GNP-sLe^x** particle identification using post mortem immunohistochemical (anti-FITC) detection (Fig. 4 *A–D*); anti-FITC-HRP staining of tissue slices from the animals tested showed the presence of the particles in the activated hemisphere even after perfusion of the animal. Moreover, the targeted localization of larger particles in the size-range of 1 μm could even be detected by eye (Fig. 4*D*).

In conclusion, it has been demonstrated that the SCM precursor group can be used as a highly versatile, early-introduced, chemical linker system for the synthesis of amine-reactive complex carbohydrate reagents. Suitable amine-coated magnetic nanoparticles (NPs) when reacted with such reagents can be chemically decorated with key biomarker ligands such as sialyl Lewis^X (sLe^X) and as a result have shown excellent targeting to activated endothelium. The good correlation observed here between the in vitro data for those particles that bind well to E-selectin (**GNP-sLe^x** and **GNP-sLe^x-FITC**) and those that do not (**NP** and **GNP-LacNAc**) with the binding observed in vivo presented suggests that this may be mediated by expressed selectin biomarkers; use of anti-E-selectin antibodies shows up-regulation at targeted inflamed tissue sites and future experiments will delineate other possible correlations with selectin binding. The resulting **GNP-sLe^X** constructs are highly sensitive (even to single particle detection) and selective T_2 contrast agents for detecting the natural molecular interactions underlying leukocyte and T cell recruitment to the brain in neuropathology and have been validated here in clinically-relevant disease models. Previous strategies (54, 55) for targeting selectins as biomarkers have shown lower sensitivities (54), high background signals (55), and more restrictive temporal windows (55); these suggest important roles for the use of a proven, natural small molecule ligand (sLe^X) and high ligand copy number attached to a particle of controllable size in the success of the **GNP-sLe^X** system. The use of **GNP-sLe^X** containing endogenous small molecule ligands for the detection of target protein biomarkers also allows here the advantage of transferable cross-species utility that is more difficult to achieve with antibody-mediated binding (2, 55). It should be noted that **GNP-sLe^X** was well tolerated in all models with no signs of ill effect or toxicity; immunohistochemical studies also revealed no evidence of ischaemia in brain or peripheral organs. Similarly, no toxicity has been observed in other conjugate (antibody) particle systems (2) even after administration of second doses. Given that simple, first-generation, unfunctionalized, high-Fe-content particles are currently undergoing approval for clinical use, with associated lack of toxicity, the development of next-generation, functional agents, such as **GNP-sLe^X**, raises the realistic and exciting possibility of their use in early, preclinical detection of MS and a host of other neuropathologies including multiinfarct dementia, HIV-associated encephalitis, or Parkinson's disease.

Materials and Methods

In Vivo Models. Adult male Wistar rats (Harlan–Olac) weighing ≈250g were anesthetized with 2.5% isoflurane in 70% N_2O:30% O_2. Using a <50-μm-tipped glass pipette, 100 ng of recombinant rat interleukin-1β (IL-1β) (NIBSC, Potters Bar) in 1 μL of saline was injected stereotaxically, 1 mm anterior and 3 mm lateral to Bregma, at a depth of 4 mm into the left striatum ($n = 6$). Animals were allowed to recover from anesthesia for ≈2.5 h, at which point they were reanesthetized as above and 500 μL of a solution containing either (*i*) **GNP-sLe^x** particles (4 mg of Fe) or (*ii*) un-modified **control-NP** particles (4 mg of Fe) was injected via a tail vein, $n = 3$ per group. A group of control animals ($n = 3$) were injected intracerebrally in the same way with 1 μL of saline alone, and subsequently with 500 μL of **GNP-sLe^x** particles (4 mg of Fe) via a tail vein ≈2.5 h later. Two additional animals were studied: the first was injected intracerebrally with 100 ng of IL-1β and systemically with **GNP-LacNAc** to verify selectivity of the **GNP-sLe^x** compared with its derivatives, and the second was injected with 10 ng of IL-1β intracerebrally followed by **GNP-sLe^x** systemically to verify that endothelial activation remained detectable with **GNP-sLe^x** at this lower dose.

After contrast agent injection, animals were positioned in a 5-cm i.d. quadrature birdcage resonator with an in-built stereotaxic frame. During MRI, anesthesia was maintained with 1.5–1.7% isoflurane in 70% N_2O:30% O_2, ECG was monitored via s.c. electrodes and body temperature was maintained at ≈37 °C with a circulating warm water system. All procedures were approved by the United Kingdom Home Office.

Disease Models. Targeted experimental allergic encephalomyelitis (EAE) lesions are induced by immunization of genetically susceptible animals with myelin proteins. This is mediated by autoimmune T cells. Three-week-old male Lewis rats (Charles River) (60–100 g) were anesthetized with 1.5–3% isoflurane in a mixture of nitrous oxide/oxygen (70%/30%) and injected s.c. at the base of the tail with a total volume of 100 μL of MOG (35–55) peptide (25 μg diluted in saline) emulsified in incomplete Freund's adjuvant (IFA; Sigma–Aldrich). For control experiments, rats were injected with the same volume of saline emulsified in incomplete Freund's adjuvant. Focal EAE lesions were induced by the stereotaxic injections of cytokines into the corpus callosum 21 days after the MOG injection. Animals were anesthetized as previously described and 2 μL of a cytokine mixture containing 1.45 μg of recombinant rat tumor necrosis factor-α (TNF-α; PeproTech) and 1 μg of recombinant rat IFN gamma (IFNγ; PeproTech) dissolved in sterile saline was injected stereotaxically at a depth of 3 mm from the cortical surface over a 10-min period. For the ET-1-stroke lesions, 200 g male wistar rats were anesthetized with 2–2.5% isoflurane in a mixture of nitrous oxide/oxygen (70%/30%), and stereotaxically injected with 10 pmoles ET-1 in 1 μL of saline in the left striatum as described in ref. 14.

Magnetic Resonance Imaging. Images were acquired using a 7T horizontal bore magnet with a Varian Inova spectrometer (Varian). A T2*-weighted 3D gradient-echo dataset encompassing the entire brain was acquired: flip angle 11°, TR = 25 ms, TE = 10 ms, matrix size 350 × 192 × 192, field of view 4.2 × 3.07 × 3.07 cm, 4 averages, total acquisition time ≈ 1h. The midpoint of the acquisition was 4.6 ± 0.4h after IL-1β or saline injection and 2.0 ± 0.4h after GNP-sLe^x or control-NP injection. Data were zero-filled to 350 × 256 × 256 and reconstructed off-line, with a final isotropic voxel size of 120 μm^3.

For the focal MOG-EAE animals, **GNP-sLe^x** was injected on day 21 after intracerebral injection of cytokines, and the 3D T2*-weighted dataset acquired 1–2h later. For the ET-1-injected animals **GNP-sLe^x** was injected 1h after intracerebral injection of ET-1, and the 3D T2*-weighted dataset acquired 1.5–2.5h later. In both the MOG-EAE and ET-1 models, CBV maps were obtained from a time series of gradient echo images (TR = 20 ms, TE = 10 ms, flip angle = 20°, 128 × 64 matrix, 5 × 4 cm FOV) during bolus injection of the intravascular contrast agent gadolinium-DTPA-BMA (Gd[DTPA/BMA] Omniscan) (56). T_1-weighted images were acquired using a spin-echo sequence (TR = 500 ms, TE = 20 ms, 128 × 64 matrix, 5 × 5 cm FOV) both before and 10 min after contrast agent injection to ensure BBB integrity.

Segmentation and Volumetric Quantification. In each MR image the brain was masked manually to exclude extracerebral structures. Areas of low signal were segmented. To control for minor variations in absolute signal intensity between individual scans, low signal areas were calibrated on 10 evenly spaced slices per brain. The median signal intensity value was then applied to signal intensity histogram-based fully automated batch analysis of the entire sequence. In this way, masks were generated corresponding to areas that were both within the brain and of defined low signal intensity. Segmentation and volumetric quanti-

fication were undertaken using ImagePro Plus software (version 4.5.1, Media Cybernetic) by an operator blinded to the origin of all data.

Immunolocalisation of Fluorescein. Frozen, 20-μm-thick serial coronal sections were cut through the microinjection site in the IL-1β-challenged brain. Fluorescein was identified by immunohistochemistry using standard procedures. Briefly, tissue sections were fixed for 20 min in 100% cold ethanol, endogenous peroxidases were blocked for 20 min (0.3% H_2O_2 in methanol) and F_c receptors blocked for 60 min (10% normal goat serum). A biotinylated anti-fluorescein antibody (Vector Laboratories) was then applied to the sections (5 mg/ml) and incubated overnight at room temperature before detection using a standard ABC amplification system (Vector Laboratories). Negative controls were incubated without antibody. Immunopositivity was revealed with diaminobenamidine (Vector Laboratories) in the presence of the catalyst imidazole (0.01M). Tissue sections were counterstained with cresyl-violet.

ACKNOWLEDGMENTS. We thank Andrew Lowe for technical assistance. This work was supported by a studentship from Glycoform Ltd. (to S.I.v.K. and B.G.D.), Medical Research Council Grant G0400131 (to N.R.S. and S.S.), and Cancer Research United Kingdom Grant C28462/A10158 (to N.R.S.).

1. Tsourkas A, *et al.* (2005) In vivo imaging of activated endothelium using an anti-VCAM-1 magnetooptical probe. *Bioconjugate Chem* 16:576–581.
2. McAteer MA, *et al.* (2007) In vivo magnetic resonance imaging of acute brain inflammation using microparticles of iron oxide. *Nat Med* 13:1253–1258.
3. Cayrol R, *et al.* (2008) Activated leukocyte cell adhesion molecule promotes leukocyte trafficking into the central nervous system. *Nat Immunol* 9:137–145.
4. Lee BPL, Imhof BA (2008) Lymphocyte transmigration in the brain: A new way of thinking. *Nat Immunol* 9:117–118.
5. Sibson NR, *et al.* (2004) MRI detection of early endothelial activation in brain inflammation. *Magn Reson Med* 51:248–252.
6. Barber PA, *et al.* (2004) MR molecular imaging of early endothelial activation in focal ischemia. *Ann Neurol* 56:116–120.
7. Boutry S, *et al.* (2005) Magnetic resonance imaging of inflammation with a specific selectin-targeted contrast agent. *Magn Reson Med* 53:800–807.
8. Weissleder R, Kelly K, Sun EY, Shtatland T, Josephson L (2005) Cell-specific targeting of nanoparticles by multivalent attachment of small molecules. *Nat Biotechnol* 23:1418–1423.
9. Gasser DL, Newlin CM, Palm J, Gonatas NK (1973) Genetic control of susceptibility to experimental allergic encephalomyelitis in rats. *Science* 181:872–873.
10. Williams RM, Moore MJ (1973) Linkage of susceptibility to experimental allergic encephalomyelitis to the major histocompatibility locus in the rat. *J Exp Med* 138:775–783.
11. Martin R, McFarland HF McFarlin DE (1992) Immunological aspects of demyelinating diseases. *Annu Rev Immunol* 10:153–187.
12. Sharkey J, Ritchie IM, Kelly PAT (1993) Perivascular microapplication of endothelin-1: A new model for focal cerebral ischemia in the rat. *J Cereb Blood Flow Metab* 13:865–871.
13. Sharkey J, Butcher SP (1995) Characterisation of an experimental model of stroke produced by intracerebral microinjection of endothelin-1 adjacent to the rat middle cerebral artery. *J Neurosci Methods* 60:125–131.
14. Sibson NR, *et al.* (2008) Acute astrocyte activation in brain detected by MRI: New insights into T1 hypointensity. *J Cereb Blood Flow Metab* 28:621–632.
15. Von Andrian, U. H. Mackay, C. R. T-cell function and migration: Two sides of the same coin (2000) *N Engl J Med* 343:1020–1034.
16. Halkes KM, Carvalho De Souza A, Maljaars CEP, Gerwig GJ, Kamerling JP (2005) A facile method for the preparation of gold glyconanoparticles from free oligosaccharides and their applicability in carbohydrate-protein interaction studies *Eur J Org Chem* 3650–3659.
17. Carvalho De Souza A, *et al.* (2005) Gold glyconanoparticles as probes to explore the carbohydrate-mediated self-recognition of marine sponge cells. *ChemBioChem* 6:828–831.
18. Carvalho De Souza A, *et al.* (2004) Synthesis of gold glyconanoparticles: Possible probes for the exploration of carbohydrate-mediated self-recognition of marine sponge cells. *Eur J Org Chem* 4323–4339.
19. De la Fuente JM, *et al.* (2001) Gold glyconanoparticles as water-soluble polyvalent models to study carbohydrate interactions. *Angew Chem Intl Ed* 40:2258–2261.
20. De La Fuente JM, Penades S (2005) Glyco-quantum dots: A new luminescent system with multivalent carbohydrate display. *Tetrahedron Asymmetry* 16:387–391.
21. De La Fuente JM, Penades S (2004) Understanding carbohydrate-carbohydrate interactions by means of glyconanotechnology. *Glycoconjugate J* 21:149–163.
22. Derfus AM, Chan WCW, Bhatia SN (2004) Probing the cytotoxicity of semiconductor quantum dots. *Nano Lett* 4:11–18.
23. Schlenoff JB, Li M, Ly H (1995) Stability and self-exchange in alkanethiol monolayers. *J Am Chem Soc* 117:12528–12536.
24. Zhao Y, Perez-Segarra W, Shi Q, Wei A (2005) Dithiocarbamate assembly on gold. *J Am Chem Soc* 127:7328–7329.
25. Flynn NT, Tran TNT, Cima MJ, Langer R (2003) Long-term stability of self-assembled monolayers in biological media. *Langmuir* 19:10909–10915.
26. Tanaka H, Ando Y, Wada M, Takahashi T (2005) Synthesis of DTPA-conjugated (1,4)-linked 2-aminoglycosides varying in the anomeric configuration and their MRI contrast effect. *Org Biomol Chem* 3:3311–3328.
27. Andre JP, *et al.* (2004) Lanthanide(III) complexes of DOTA-glycoconjugates: A potential new class of lectin-mediated medical imaging agents. *Chem Eur J* 10:5804–5816.
28. Fulton DA, *et al.* (2006) Glycoconjugates of gadolinium complexes for MRI applications. *Chem Commun.* 1064–1066.
29. Takahashi M, *et al.* (2000) Utilization of dendritic framework as a multivalent ligand: A functionalized gadolinium(III) carrier with glycoside cluster periphery. *Tetrahedron Lett* 41:8485–8488.
30. Baia P, *et al.* (2005) Lanthanide(III) chelates of DTPA bis(amide) glycoconjugates: Potential imaging agents targeted at the asyaloglycoprotein receptor. *Eur J Inorg Chem* 2110–2119.
31. Lundquist JJ, Toone EJ (2002) The cluster glycoside effect. *Chem Rev* 102:555–578.
32. Lee YC (1992) Biochemistry of carbohydrate-protein interaction. *FASEB J* 6:3193–3200.
33. Lee YC, Lee RT (1995) Carbohydrate-protein interactions: Basis of glycobiology. *Acc Chem Res* 28:321–326.
34. Mammen M, Choi SK, Whitesides GM (1998) Polyvalent interactions in biological systems: Implications for design and use of multivalent ligands and inhibitors. *Angew Chem Intl Ed* 37:2754–2794.
35. Laconte L, Nitin N, Bao G (2005) Magnetic nanoparticle probes. *Materials Today* 8:32–38.
36. Bulte JWM, Kraitchman DL (2004) Iron oxide MR contrast agents for molecular and cellular imaging. *NMR Biomed* 17:484–499.
37. Josephson L, Tung CH, Moore A, Weissleder R (1999) High-efficiency intracellular magnetic labeling with novel superparamagnetic-tat peptide conjugates. *Bioconjugate Chem* 10:186–191.
38. Bulte JWM, *et al.* (1999) Neurotransplantation of magnetically labeled oligodendrocyte progenitors: Magnetic resonance tracking of cell migration and myelination. *Proc Natl Acad* Sci 96:15256–15261.
39. Perez JM, O'Loughin T, Simeone FJ, Weissleder R, Josephson L (2002) DNA-based magnetic nanoparticle assembly acts as a magnetic relaxation nanoswitch allowing screening of DNA-cleaving agents. *J Am Chem Soc* 124:2856–2857.
40. Palmacci S, Josephson L, Groman EV (1995). US 76829505669 (Advanced Magnetics).
41. Chan WC, White PD (2000) *Fmoc Solid Phase Peptide Synthesis* (Oxford Univ Press, Oxford).
42. Lee YC, Stowell CP, Krantz MJ (1976) 2-Imino-2-methoxyethyl 1-thioglycosides: New reagents for attaching sugars to proteins. *Biochemistry* 15:3956–3963.
43. Pearce OMT, *et al.* (2005) Glycoviruses: Chemical glycosylation retargets adenoviral gene transfer. *Angew Chem Intl Ed* 44:1057–1061.
44. Robinson MA, *et al.* (2004) LEAPT: Lectin-directed enzyme-activated prodrug therapy. *Proc Natl Acad Sci USA* 101:14527–14532.
45. Stowell CP, Lee YC (1982) Preparation of neoglycoproteins using 2-imino-2-methoxyethyl 1-thioglycosides. *Methods Enzymol* 83:278–288.
46. Sobenin IA, Tertov VV, Orekhov AN (1998) Optimization of the assay for sialic acid determination in low density lipoprotein. *J Lipid Res* 39:2293–2299.
47. Udenfrlend S, *et al.* (1972) Fluorescamine: A reagent for assay of amino acids, peptides, proteins, and primary amines in the picomole range. *Science* 178:871–872.
48. Dwek RA, Edge CJ (1993) Analysis of glycoprotein-associated oligosaccharides. *Annu Rev Biochem* 62:65–100.
49. Nelson RM, Dolich S, Aruffo A, Cecconi O, Bevilacqua MP (1993) Higher-affinity oligosaccharide ligands for E-selectin. *J Clin Investigation* 91:1157.
50. Bernardes-Silva M, Anthony DC, Issekutz AC, Perry VH (2001) Recruitment of neutrophils across the blood–brain barrier: The role of E- and P-selectins. *J Cereb Blood Flow Metab* 21:1115–1124.
51. Anthony DC, Bolton SJ, Fearn S, Perry VH (1997) Age-related effects of interleukin-1β on polymorphonuclear neutrophil-dependent increases in blood–brain barrier permeability in rats. *Brain* 120:435–444.
52. Blamire AM, *et al.* (2000) Interleukin-1b-induced changes in blood–brain barrier permeability, apparent diffusion coefficient, and cerebral blood volume in the rat brain: A magnetic resonance study. *J Neurosci* 20:8153–8159.
53. Sibson NR, *et al.* (2007) Acute astrocyte activation in brain detected by MRI: New insights into T1 hypointensity *J Cereb Blood Flow Metab.*
54. Boutry S, Laurent S, Elst LV, Muller RN (2006) Specific E-selectin targeting with a superparamagnetic MRI contrast agent. *Contrast Med Mol Imaging* 1:15–22.
55. Reynolds PR, *et al.* (2006) Detection of Vascular Expression of E-selectin in Vivo with MR-Imaging. *Radiology* 241:469–476.
56. Sibson NR, *et al.* (2002) TNF-{alpha} reduces cerebral blood volume and disrupts tissue homeostasis via an endothelin- and TNFR2-dependent pathway. *Brain* 125:2446–2459.